Post-Print:IEEE Trans. Electron Devices, Vol. 59, No. 12, p3327 (2012). DOI 10.1109/TED.2012.2216535.

Buffer Design to Minimize Current Collapse in GaN/AlGaN HFETs

Michael J. Uren, *Member, IEEE*, Janina Möreke, and Martin Kuball

***Abstract*—The bulk trap induced component of current collapse in GaN/AlGaN HFETs is studied in drift diffusion simulations, distinguishing between acceptor traps situated in the top and bottom half of the bandgap, with Fe and C used as specific examples. It is shown that Fe doping results in an inherent but relatively minor contribution to dispersion under pulse conditions. This simulation is in reasonable quantitative agreement with double pulse experiments. Simulations using deep-level intrinsic growth defects produced a similar result. By contrast, carbon can induce a strong current collapse which is dependent on doping density. The difference is attributed to whether the trap levels, whether intrinsic or extrinsic dopants, result in a resistive n-type buffer or a p-type floating buffer with bias dependent depletion regions. This insight provides a key design concept for compensation schemes needed to ensure semi-insulating buffer doping for either RF or power applications.**

***Index Terms*—Dispersion, DIVA, HEMT, Pulse IV**

I. Introduction

HETEROJUNCTION field effect transistors (HFETs) based on the GaN/AlGaN materials system offer outstanding performance, with RF power density exceeding 30W/mm [1]. One issue which has limited RF power and therefore has received extensive research is "DC-RF dispersion" or "current-collapse" (CC). This results in the device delivering lower RF power than would be expected from the DC I_d-V_{ds} device characteristic. Similar issues occur in power devices where the problem appears as an increase in dynamic on-resistance. Two sources of dispersion have been identified. The first, and most intensively studied, is due to surface effects associated with localized and reversible charge trapping in defects located near the corner of the gate resulting in a "virtual gate" which reduces the current handling of the channel and leads to "knee-walkout" [2-4]. The second mechanism and the subject of this article, is the result of charge trapping in deep levels within the semi-insulating buffer [2]. Buffer related CC was explained in a generic way as being due to hot-carrier injection into the buffer followed by trapping in deep levels. These deep levels are a necessary requirement for device operation since they suppress buffer leakage and short-channel effects[5]. The GaN buffer was originally rendered insulating using intrinsic growth defects and this approach has continued to deliver outstanding device performance [6]. Extensive simulations of such buffers have shown that charge trapping in compensated intrinsic deep donors and acceptors can result in CC which varies with geometry, buffer doping, and trap energy level [7-9]. Although these simulations have clearly demonstrated a bulk GaN CC effect, they have not been linked to experiment, and the detailed mechanism has not been clearly described.

More recent GaN/AlGaN HFET devices have often preferred to use extrinsic deep level dopants to make the buffer insulating, partly due to the ease of monitoring and control during growth. Although we consider intrinsic defects, here we concentrate on extrinsic dopants with energy levels in the upper and lower part of the bandgap, considering two widely used dopants, iron (Fe) and carbon (C). Fe has been successfully employed to render the buffer semi-insulating [10-13] and deliver the highest RF power [1]. There is some inconsistency in the literature, one report of CC in devices with Fe buffers showed only small CC and little change with varying Fe doping [11], whereas reference [14] found that Fe led to strong CC. C is an alternative deep acceptor and has been intentionally introduced as a route to an insulating buffer [12, 15]. C related defects have also been identified as the deep acceptor in intrinsic buffers [16]. The C has been shown to produce a strong CC when incorporated in the vicinity of the channel, but nevertheless has given excellent isolation and power device performance [12, 13].

To quantify the CC, rather than measure RF dispersion or efficiency, the dynamic *I-V* analysis (DIVA) double pulse measurement technique is often used [17]. This technique involves fast pulsed measurements from a quiescent bias corresponding to the RF operating point to all parts of the IV plane, and is generally well correlated with RF dispersion [3, 13]. In this work, the full DIVA measurement is simulated and used to examine the buffer contribution to the dispersion. The effect of different buffer doping combinations is considered in detail. It is shown that back gating is the principal cause of buffer related CC in Fe doped as well as most intrinsic buffers. Why CC is minimized and largely independent of dopant density is explained by Fermi-level pinning in the upper half of the bandgap making the buffer n-type. It is also shown that any floating p-type buffer such as carbon doped GaN can

Manuscript received July 16, 2012, revised August 22, 2012, accepted August 23, 2012. This work was supported by the U.K. Engineering and Physical Sciences Research Council grant EP/I033165/1. We would like to thank H. Jung of UMS for the devices.

The authors are with the H. H. Wills Physics Laboratory, Tyndall Avenue, University of Bristol, Bristol BS8 1TL, U.K. (e-mail: Michael.uren@bristol.ac.uk, janina.moereke@bristol.ac.uk, martin.kuball@bristol.ac.uk).

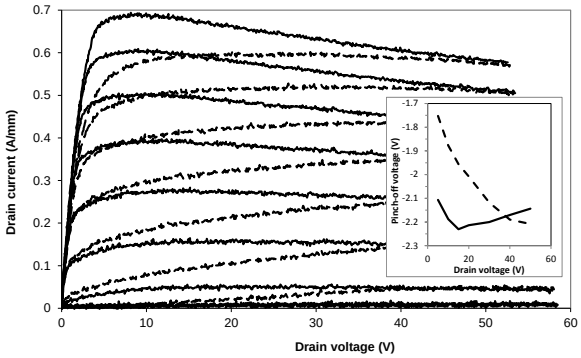

Fig. 1. Pulsed I-V measurement of Fe doped FET with 1µs long and 1ms separation pulses. Solid black: pulsed from quiescent bias of V_{gs}=0V, V_{ds}=0V, dashed: pulsed from V_{gs}=-3V, V_{ds}=40V. V_{gs} is -3 to +1V in 0.5V steps. Inset shows the shift in pinch-off voltage.

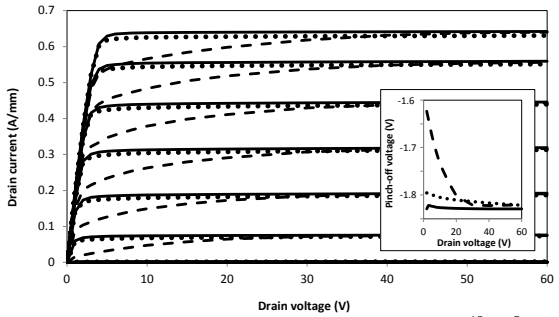

Fig. 2. Simulated pulse IV with Fe doped buffer with $3x10^{18}cm^{-3}$ in the bulk, then falling exponentially at 0.4µm/decade to $3.6x10^{16}cm^{-3}$ at the surface. Solid black, pulsed from V_{gs}=0V, V_{ds}=0V, dashed pulsed from V_{gs}=-3V, V_{ds}=40V. Dotted line is a simulated DC sweep. Inset shows the shift in pinch-off voltage.

result in serious CC. Reasonable quantitative agreement of the simulations with experimental DIVA data is demonstrated for Fe doped devices.

II. Simulations

The Silvaco ATLAS 2D drift-diffusion simulator was used to model the device response, based on an earlier simulation of the virtual gate effect[3]. A standard reference silicon nitride passivated AlGaN/GaN-on-SiC HFET was considered for all simulations, with 0.5µm long T gate and 6µm source-drain gap. The source and drain contacts to the channel were implemented using heavily doped GaN regions with the mobility adjusted to give 0.2Ωmm contact resistance. The device contained an undoped 25nm thick AlGaN layer on a 1.4µm thick GaN buffer, on SiC. The charge at the AlGaN surface was set to zero corresponding to exact compensation of the polarization charge by surface donors, and an absence of any virtual gate charge. The polarization charge at the GaN/AlGaN interface and GaN mobility were adjusted to give reasonable agreement in DC transconductance and pinch-off voltage with a reference device (shown in Fig. 1) and then were kept fixed. The nucleation layer was not modeled. Self-heating was not enabled to focus solely on electrical trap induced time dependence rather than adding an additional and potentially confusing thermal time dependent behavior. Shockley-Read-Hall and Fermi-Dirac statistics were enabled, but not impact ionization or gate tunneling, effectively excluding all surface or gate related effects from the simulation. The buffer doping was varied using a wide range

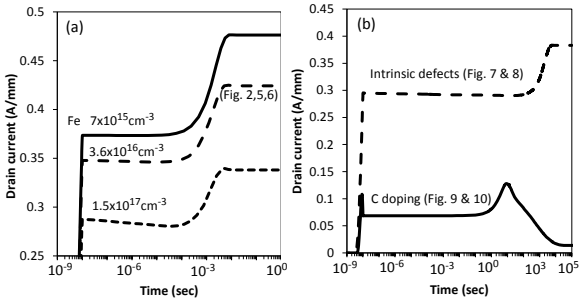

Fig. 3. Simulated drain current transients for GaN buffer doping distributions following a voltage step from V_{ds}=40, V_{gs}=-3V to V_{ds}=5, V_{gs}=0V. The ramptime is 10ns. (a) Fe surface concentration is as indicated, rising at 0.4µm per decade to a bulk doping of $3x10^{18}cm^{-3}$. (b) Intrinsic growth defects and the C doping distribution of Figs 7 to 10.

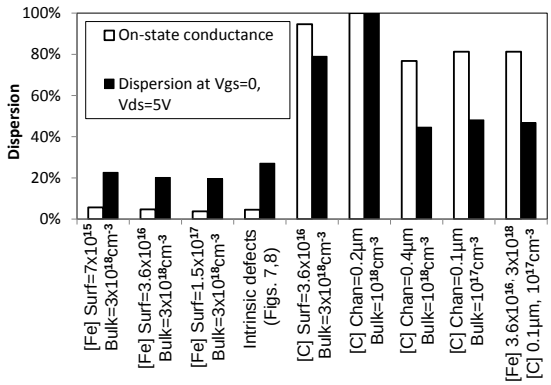

Fig.4. Simulated dispersion 1µs after pulse between quiescent biases of V_{ds}=40, V_{gs}=-3V and V_{ds}=0, V_{gs}=0V for a representative set of doping profiles. Open bars: fall in on-state conductance at V_{ds}=1V, V_{gs}=1V. Solid bars: fall in current at V_{ds}=5, V_{gs}=0V.

of Fe and C deep-acceptor, or intrinsic deep donor/acceptor doping distributions. The impact of multiple acceptor/donor states is described in books such as [18]. In all cases the deep level capture cross-section was set to a typical value of $10^{-15}cm^2$ for capture into neutral states and $10^{-13}cm^2$ for Coulomb attractive capture[19]. All simulations also included a low density ($10^{15}cm^{-3}$) of shallow compensating donors. All distributions studied had sufficiently high doping to suppress significant short-channel effects[5], so that they all showed similar DC *I-V* characteristics, only differing in the pinch-off voltage.

III. Fe Doping: Measurement and Simulation

Fig. 1 shows the experimental pulsed *I-V* DIVA characteristic for a Fe doped device with the same design as simulated. Here the solid and dashed curves correspond to pulsing to all points on the *I-V* plane from the unbiased open-channel quiescent point (V_{ds}=0, V_{gs}=0V) and the class B RF operating point (V_{ds}=40, V_{gs}=-3V) respectively. The 1µs pulse duration is sufficiently fast to remove most self-heating effects [20] but some residual heating is still present resulting in the negative output conductance. This device showed almost none of the knee-walkout characteristic of virtual gate effects, suggesting minimal surface trapping [3]. However there was dispersion between the two pulse operating points. The pulsed measurement from the class B quiescent point showed a current reduction which was dependent on the size of the

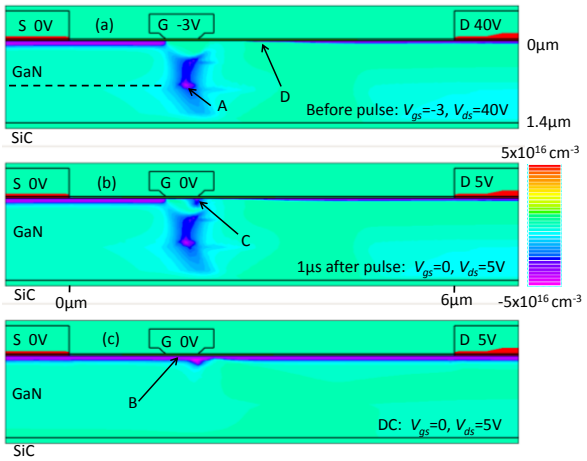

Fig. 5. Net dopant charge density in the GaN (a) before, (b) after the pulse, and (c) at equilibrium. Fe doped with 3.6x10^{16} at surface rising to 3x10^{18}cm^{-3} in bulk (marked with dashed line).

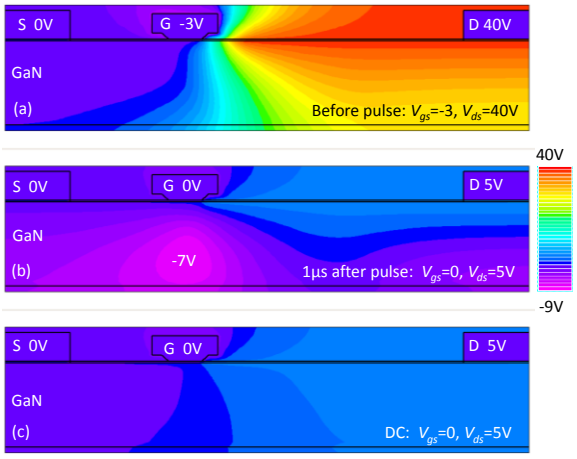

Fig. 6. Conduction band energy, doping as in Fig. 5.

negative step in drain potential. This fall in current was due to a pulsed drain-voltage dependent shift in pinch-off voltage which occurred on a timescale shorter than the 1µs pulse duration (inset to Fig. 1). There was a 15% change in the on-state conductance. The pinch-off shift linked CC behavior shown here has been seen on a wide variety of device technologies from many sources.

Fig. 2 shows simulated DIVA characteristics for a Fe doped device for the same operating points as in Fig. 1. Each set of I-V curves is constructed from 135 transient simulations where the current shown is the simulated current 1µs after a 10ns ramp from the equilibrium quiescent bias to each pulse bias. Fe is incorporated into GaN during growth by a surface segregation mechanism [21], so the density was taken to be constant in the bulk of the GaN and then to fall exponentially towards the surface at 0.4µm/decade following the turn-off of the Fe doping source. The surface Fe density was varied in different simulations between 7x10^{15} and 1.5x10^{17}cm^{-3} by varying the turn-off depth from 1.1 to 0.5µm. The bulk GaN Fe density varied between 10^{17} and 3x10^{18}cm^{-3}. These surface densities correspond to those reported in [11]. A single acceptor energy level 0.5eV below the conduction band was used for Fe based on the experimental evidence that the Fermi level is pinned at this energy [22] and the Fe^{2+}/Fe^{3+} acceptor level is the dominant recombination path [23].

It is clear that the simulation has captured the dispersive characteristics of the DIVA measurement in Fig. 1 with both qualitative and reasonable quantitative agreement. There was only a small increase in on-resistance (about 5%) and a similar magnitude shift in pinch-off voltage to the measurements (see inset to Fig. 2). Very interestingly, there was only a small variation in dispersion for varying Fe doping profile (see Fig. 4). Fig. 3a shows the simulated drain transient for three different Fe doping distributions. Following the ramp, there was a small reduction in current whose rate was roughly constant with log time and dependent on surface doping density. However the principal effect was the larger increase in current to reach the final equilibrium level after about 1ms.

IV. Model and Discussion: Fe Doped Buffer

It is important to discuss in some detail the mechanisms for the current transient shown in Fig. 3a, since this most closely corresponds to the situation which pertains in RF-CC. Since the Fe trap level pins the Fermi level in the upper half of the 3.4eV bandgap, holes essentially take no part in the operation of the device and the buffer acts like a very weakly conducting n-type layer with small surface depletion regions. The dispersion seen in Figs. 3a requires that there is a change in the distribution of trap charge on both short and long timescales from the end of the pulse through to the final equilibrium state. To explain this we must identify where the charge is stored as a function of time and its charge/discharge mechanism. Fig. 5 shows the net ionized dopant charge in the buffer at equilibrium before the pulse, 1µs after the ramp, and in the final static state. Fig. 6 displays the corresponding potential distribution. The dispersion arises as a result of the change in charge density between Figs. 5b and 5c.

There are four relevant regions where charge is stored and indicated in Fig. 5. Regions A and D are respectively net negative and positive charged (region D is a thinning of the surface depletion region and is net positive as a result of the positive interface polarization charge and the low electron density in this region, neither of which are shown here) and support the drain electric field between the gate region and the drain extension at the class B operating point. The size of the space charge A is set by the gate-drain capacitance and so is largely independent of Fe doping density, and is just a function of quiescent drain bias and device geometry provided the acceptor density exceeds this charge density. This charge is also responsible for the suppression of short-channel effects. As seen later and crucially for the CC mechanism, it screens the field and results in a potential close to zero in region A prior to the pulse (Fig. 6a). Region B is the charge stored in a depletion region under the gate itself, and is a function of the change in gate bias during the pulse ie a “gate lag” effect. Initially it is uncharged. Region C is charge injected into the buffer in the vicinity of the drain end of the gate. This region is initially uncharged for the situation shown in Fig. 5a where

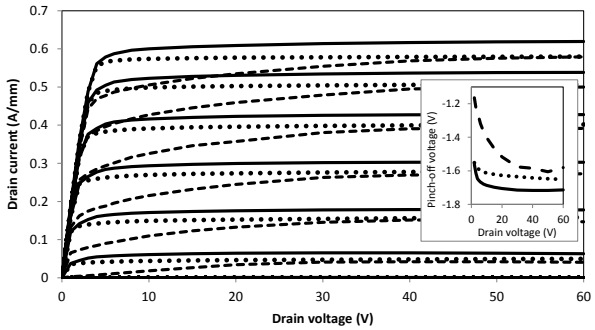

Fig. 7. Simulated pulsed IV for intrinsic defect doped buffer. Solid line pulsed from V_{ds}=0, V_{gs}=0V, dotted line DC-IV, dashed line, pulsed from V_{ds}=40, V_{gs}=-3V. 10^{15}cm^{-3} shallow donor, 10^{17}cm^{-3} deep donor 1eV below the conduction band, and 5x10^{16}cm^{-3} deep acceptor 0.6eV above the valence band.

only deep acceptors are present. During the ramp, the barrier is lowered so region C is negatively charged by electron injection from the channel, as is apparent in Fig. 5b. However after the ramp there is no further significant change in this region with time and so it makes no contribution to the dispersion.

Following the pulse, region B results in the small acceptor density dependent drop in current with time seen in Fig 3a. Electron capture from the channel into the acceptors under the gate occurs as the depletion region gradually re-forms leading to the change in charge distribution seen between Fig. 5b and 5c and a small negative pinch-off voltage shift with time.

The largest contribution to the dispersion comes from region A. After the pulse to a more negative bias, the charged acceptor traps in region A under the middle of the gate have an integrated net charge of -2.3x10^{12}cm^{-2}. They are isolated from the channel by a potential barrier and cannot immediately change their charge state. The buffer acts like a dielectric superimposing the potential due to capacitive coupling between the contacts onto the underlying stored quiescent potential background. Following the pulse, this results in a potential under the gate in region A which is more negative the larger the negative step in drain potential. For the conditions of Fig 5b, region A is at -7V. This back-bias results in a drop in channel charge of about 4x10^{11}cm^{-2} and a positive threshold shift of about 0.2V. This is the origin of the bias dependent pinch-off voltage shift seen in Fig. 2. Eventually thermal emission empties the acceptors in region A and leads to the large step in current to be seen in Fig. 3a as the device returns to equilibrium. In the situation where the drain bias is pulsed to a more positive voltage, for the Fe doped device the barrier is only 0.5eV so the buffer is easily forward biased relative to the channel allowing electrons to be injected into region A and allowing the potential to reach equilibrium in less than the 1 µs measurement time. This explains why pulsing to more positive voltages in Figs. 1 and 2 shows little dispersion.

It is important to note that most of the charge storage occurs under the gate resulting in a transient pinch-off voltage shift with only small change in the source or drain resistance.

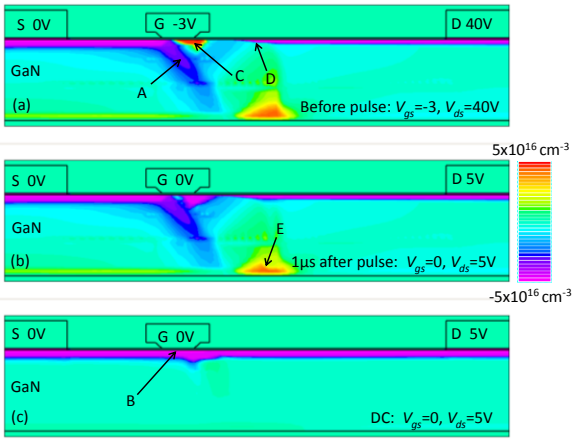

Fig. 8. Net dopant charge density in the GaN before and after a pulse. Intrinsic dopants are as in Fig. 7.

V. Model and Discussion: Intrinsic Buffers

Buffers which are made semi-insulating using intrinsic growth defects are believed to have a deep donor in the upper half of the gap and a deep acceptor in the lower half of the 3.4eV gap[24]. Provided the donor density exceeds the acceptor density, this pins the Fermi level near the donor level [9, 18]. We used a deep donor density of 10^{17}cm^{-3} at energy level 1.0eV below the conduction band and a deep acceptor density of 5x10^{16}cm^{-3} at an energy level 0.6eV above the valence band, similar to [9].

The results are shown in Figs. 7 and 8. The dispersion simulated is similar in size to that shown in [9], but the device simulation results in a much lower access resistance and an *I-V* characteristic which is much closer to that normally measured. The pulse *I-V* dispersive behavior in Fig. 7 is similar to that shown in Figs. 1 and 2. Not surprisingly the dispersion had a much longer time constant for the eventual return to equilibrium given the deeper Fermi pinning energy, as can be seen in Fig. 3b. The principal difference in the charge distribution resulting from the presence of deep donors as well as acceptors occurred in the quiescent charge distribution at the class B operating point prior to the pulse. Fig. 8a shows that region C was initially charged positive (rather than being neutral as in Fig. 5a). During the pulse itself, this net positive donor charge was neutralized by the injection of electrons from the channel resulting in a negatively charged region C as before (Fig. 8b) which did not change any further (Fig. 8c), meaning that it had no effect on the dispersion. Another minor difference was that there was an additional positively charged region E in the vicinity of the GaN/SiC interface. Following the pulse, the trapped charge distribution was similar to the Fe doped case, with trapped negative charge under the gate in region A. The difference in the shapes of region A reflect the fact that in Fig. 5 the doping increases exponentially with depth below the surface whereas it is constant in Fig. 8. The same back-bias mechanism described in the previous section led to the dispersion, with the potential under the gate being -6V after the pulse. As can be seen in Fig. 4, the size of the dispersion in both drain current and on-conductance was remarkably similar to that seen for Fe

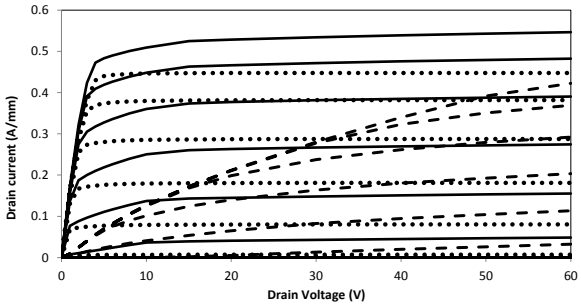

Fig. 9. Simulated pulsed IV for C doped buffer with the same doping profile as Fig. 2. Solid line pulsed from V_{ds}=0, V_{gs}=0V, dotted line DC-IV, dashed line pulsed from V_{ds}=40, V_{as}=-3V.

doping, despite the dramatic differences in trap distribution, reflecting the geometric origin of the space charge.

VI. Impact of Carbon Doping

As a next step, in contrast to Fe or intrinsic doping where the Fermi level lies in the upper half of the conduction band, an energy state in the lower half of the conduction band was considered using the example of C doping. Unlike Fe, carbon doping does not suffer from any memory effect during growth so discontinuous changes in C doping profile are possible. Such profiles with thin undoped channel regions were reported in [12, 13] and both found that this was necessary to reduce CC. C doping profiles with bulk C density between 10^{17} and 10^{18}cm^{-3} were simulated with an undoped channel region of 100-400nm thickness. Carbon has an acceptor level which is reported to be located about 0.9eV above the valence band [25] and so providing its density exceeds that of any donor states, the Fermi level will be located near this energy in the lower half of the gap and the material will be p-type.

To allow direct comparison with the results for Fe doping, a device was simulated with the same exponential distribution of C as was employed in Fig. 2 for Fe, and this is shown in Fig. 9. Since the p-type buffer is isolated from the channel by depletion regions, the buffer is floating, although the simulation assumes that the floating buffer is at true equilibrium before the pulse. The complex transient behavior out to 10^5s is shown in Fig. 3b. There was a dramatic increase in dispersion compared to Fe doping, with an enormous fall in the on-conductance when pulsed from the class-B operating point, in some cases leading to complete pinch-off. All C doped profiles simulated resulted in increased dispersion and on-conductance with a strong dependence on doping profile. Representative results are shown in Fig. 4.

The origin of the strong dispersion is clear from Fig. 10, which shows the potential distribution before and after the pulse. Prior to the pulse under class-B static conditions, the p-n junction under the drain was reverse biased and the p-n junction under the source slightly forward biased resulting in the buffer having an equipotential at close to zero volts (Fig. 10a). Following the pulse (Fig. 10b), the low conductivity of the buffer, the capacitive coupling between the terminals and the inability of the deep levels to change their charge state meant that the buffer under the drain was forced to a potential equal to the size of the negative voltage step, in this case -35V. This large back bias under the entire gate-drain region reduced the channel charge in the ungated region and dramatically increased the transient drain resistance. After 10^5s the floating buffer came to an equipotential of -15V (Fig. 10c) resulting in a large increase in source as well as drain resistance (see Fig 3b), but in the absence of any significant source of holes, this floating buffer potential essentially never came into equilibrium. If there were a source of holes from for instance ionizing radiation or impact ionization, then the floating buffer would eventually reach equilibrium, the depletion charge would fall and the on-conductance return to a high value.

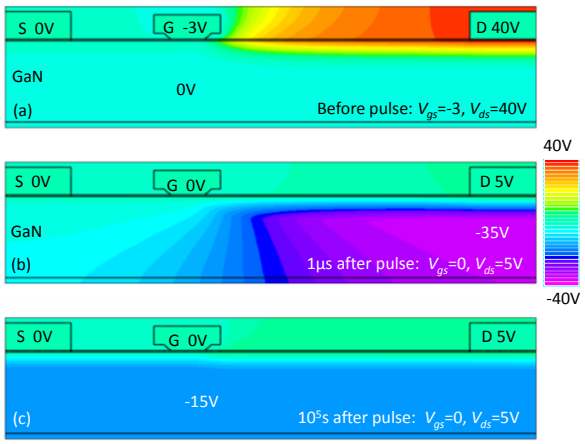

Fig. 10. Conduction band energy in the GaN before, and 1µs and 10^5s after a pulse. C doping profile is as in Fig. 9.

In reality, C is a common contaminant in MOCVD growth so it is likely that Fe doped buffers will also include C [16]. Hence co-doped buffers were also simulated. It was found that for co-doped buffers of any Fe density where the C concentration exceeded that of any shallow donors present, the simulated dispersion was very large and characteristic of the C doping. The result of one such co-doping simulation is shown in Fig. 4. These results are consistent with the fact that such co-doped GaN will have the Fermi level pinned near the C level independent of Fe density and will have a p-type floating buffer. We can speculate that this co-doping effect could explain the poor CC seen for Fe doped devices in [14].

The long time constants associated with the wide bandgap of GaN and a floating p-type GaN buffer will make the pulse dispersion highly bias history dependent. Only a single pulse has been simulated whereas the real measurement uses multiple pulses. Also the assumption here is that the conductivity of the floating buffer is higher than the reverse biased p-n junctions allowing an equipotential to be established, however the quality of the reverse biased p-n junction may well be affected by point and extended defects. Hence it is rather difficult to predict exactly what will happen for C doped buffers, although clearly effects related to those described above are undoubtedly occurring given the strong dispersion reported in [12, 13].

VII. Conclusions

In this study the impact of a wide variety of buffer doping distributions on the bulk deep-level component of current-collapse in GaN HFETs was examined. Deep-level acceptors are essential to suppress buffer leakage, short-channel effects and punch-through. However it is shown here that associated with these acceptors is an inherent current-collapse whose magnitude is set by geometric effects and not by dopant density, provided the doping density exceeds that needed to suppress the short-channel effects. The important point is that doping schemes which use either intrinsic deep donor/deep acceptor growth defects, or doping with extrinsic impurities such as Fe, result in a buffer with the Fermi level pinned in the upper half of the gap. This means that the buffer is weakly n-type and hence largely resistive between the contacts. Nevertheless, these buffers support a geometrically determined negative space charge under the gate which screens the field associated with large drain biases, and it is the transient behavior of this space charge which leads to the bulk contribution to current collapse and not a charge injection mechanism[2]. The exact time constants for the transient response will be defect level and cross-section dependent, but the observed dispersion in DIVA measurements will be largely unaltered provided these time constants are slower than the effective measurement time.

Buffers which use very deep acceptors such as carbon, which pin the Fermi level in the lower half of the gap, are vulnerable to a very much larger current-collapse effect. This arises because the buffer is p-type and hence isolated from the channel by p-n junctions allowing it to float. Under static or quasi-equilibrium conditions large amounts of space charge can be stored under the source or drain region in the p-n junction resulting in a dramatic increase in source or drain-resistance. P-type buffers can occur even with Fe doping; any active carbon or intrinsic deep acceptor will pin the Fermi level in the lower half of the gap unless over-compensated by shallower donors. How strongly the behavior discussed here for p-type buffers actually arises will depend naturally on whether quasi-equilibrium is achieved on an operational timescale and on the quality of the drain p-n junction.

Compensation schemes for the insulating buffer in HFETs therefore should aim to achieve a Fermi level position in the upper half of the bandgap. This choice will minimize the impact of the buffer on the device characteristic under transient conditions and maximize RF power performance. Corresponding conclusions can be drawn for dynamic R_{on} in power devices.

REFERENCES

[1] Y. F. Wu, A. Saxler, M. Moore, R. P. Smith, S. Sheppard, P. M. Chavarkar, T. Wisleder, U. K. Mishra, and P. Parikh, "30-W/mm GaNHEMTs by field plate optimization," *IEEE Elec. Dev. Lett.*, vol. 25, pp. 117-119, Mar 2004.

[2] S. C. Binari, P. B. Klein, and T. E. Kazior, "Trapping effects in GaN and SiC microwave FETs," *Proc. IEEE*, vol. 90, pp. 1048-1058, 2002.

[3] C. Roff, J. Benedikt, P. J. Tasker, D. J. Wallis, K. P. Hilton, J. O. Maclean, D. G. Hayes, M. J. Uren, and T. Martin, "Analysis of DC-RF Dispersion in AlGaN/GaN HFETs Using RF Waveform Engineering," *IEEE Trans. Elec. Dev.*, vol. 56, pp. 13-19, Jan 2009.

[4] N. Braga, R. Mickevicius, R. Gaska, M. S. Shur, M. A. Khan, and G. Simin, "Edge trapping mechanism of current collapse in III-N FETs," in *Technical Digest - International Electron Devices Meeting, IEDM*, 2004, pp. 815-818.

[5] M. J. Uren, K. J. Nash, R. S. Balmer, T. Martin, E. Morvan, N. Caillas, S. L. Delage, D. Ducatteau, B. Grimbert, and J. C. De Jaeger, "Punch-Through in Short-Channel AlGaN/GaN HFETs," *IEEE Trans. Elec. Dev.*, vol. 53, pp. 395-398, 2006.

[6] S. Piotrowicz, E. Morvan, R. Aubry, E. Chartier, O. Drisse, C. Dua, M. A. diForte-Poisson, J. C. Jaequet, O. Jardel, D. Lancereau, M. Richard, N. Sarazin, S. L. Delage, D. Floriot, Z. Ouarch, S. Bansropun, T. Bouvet, T. Dean, Y. Gourdel, D. Thenot, A. J. Hydes, J. O. MacLean, G. Lecoustre, A. Martin, and T. Reveyrand, "State of the art 58W, 38% PAE X-Band AlGaN/GaN HEMTs microstrip MMIC amplifiers," in *IEEE CSIC Symposium*, 2008.

[7] K. Horio, K. Yonemoto, H. Takayanagi, and H. Nakano, "Physics-based simulation of buffer-trapping effects on slow current transients and current collapse in GaN field effect transistors," *J. Appl. Phys.*, vol. 98, p. 124502, 2005.

[8] K. Horio and A. Nakajima, "Physical Mechanism of Buffer-Related Current Transients and Current Slump in AlGaN/GaN High Electron Mobility Transistors," Jpn. J. of Appl. Phys., vol. 47, pp. 3428-3433, May 2008.

[9] K. Horio, H. Onodera, and A. Nakajima, "Analysis of backside-electrode and gate-field-plate effects on buffer-related current collapse in AlGaN/GaN high electron mobility transistors," *Jap. Appl. Phys.*, vol. 109, p. 114508, Jun 2011.

[10] S. Heikman, S. Keller, S. P. DenBaars, and U. K. Mishra, "Growth of Fe doped semi-insulating GaN by metalorganic chemical vapor deposition," *Appl. Phys. Lett.*, vol. 81, p. 439, 2002.

[11] M. J. Uren, D. G. Hayes, R. S. Balmer, D. J. Wallis, K. P. Hilton, J. O. Maclean, T. Martin, C. Roff, P. McGovern, J. Benedikt, and P. J. Tasker, "Control of short-channel effects in GaN/AlGaN HFETs," in *European Microwave Integrated Circuits Conference*, ed, 2006, pp. 65-68.

[12] C. Poblenz, P. Waltereit, S. Rajan, S. Heikman, U. K. Mishra, and J. S. Speck, "Effect of carbon doping on buffer leakage in AlGaN/GaN high electron mobility transistors," *J. Vac. Sci. Technol.*, vol. B22, p. 1145, 2004.

[13] E. Bahat-Treidel, F. Brunner, O. Hilt, E. Cho, J. Wurfl, and G. Trankle, "AlGaN/GaN/GaN:C Back-Barrier HFETs With Breakdown Voltage of Over 1 kV and Low R(ON) x A," *IEEE Trans. Elec. Dev.*, vol. 57, pp. 3050-3058, Nov 2010.

[14] V. Desmaris, M. Rudzinski, N. Rorsman, P. R. Hageman, P. K. Larsen, H. Zirath, T. C. Rodle, and H. F. F. Jos, "Comparison of the DC and microwave performance of AlGaN/GaN HEMTs grown on SiC by MOCVD with Fe-doped or unintentionally doped GaN buffer layers," *IEEE Trans. Elec. Dev.*, vol. 53, pp. 2413-2417, Sep 2006.

[15] J. B. Webb, H. Tang, S. Rolfe, and J. A. Bardwell, "Semi-insulating C-doped GaN and high-mobility AlGaN/GaN heterostructures grown by ammonia molecular beam epitaxy," *Appl. Phys. Lett.*, vol. 75, pp. 953-955, Aug 1999.

[16] P. B. Klein, S. C. Binari, K. Ikossi, A. E. Wickenden, D. D. Koleske, and R. L. Henry, "Current collapse and the role of carbon in AlGaN/GaN high electron mobility transistors grown by metalorganic vapor-phase epitaxy," *Appl. Phys. Lett.*, vol. 79, pp. 3527-3529, Nov 2001.

[17] C. P. Baylis II and L. P. Dunleavy, "Performing and analyzing pulsed current-voltage measurements," *High Frequency Electronics*, vol. May, pp. 64-69, 2004.

[18] J. Blakemore, *Semiconductor Statistics*: Pergamon Press, 1962.

[19] J. Bourgoin and M. Lannoo, *Point Defects in Semiconductors II* vol. 35: Springer-Verlag, 1983.

[20] G. J. Riedel, J. W. Pomeroy, K. P. Hilton, J. O. Maclean, D. J. Wallis, M. J. Uren, T. Martin, and M. Kuball, "Nanosecond timescale thermal dynamics of AlGaN/GaN electronic devices," *IEEE Elec. Dev. Lett.*, vol. 29, pp. 416-418, May 2008.

[21] R. S. Balmer, D. E. J. Soley, A. J. Simons, J. D. Mace, L. Koker, P. O. Jackson, D. J. Wallis, M. J. Uren, and T. Martin, "On the incorporation mechanism of Fe in GaN grown by metal-organic vapour phase epitaxy," *Phys. Stat. Sol. (c)*, vol. 3, pp. 1429-1434, 2006.

[22] A. Y. Polyakov, N. B. Smirnov, A. V. Govorkov, A. A. Shlensky, K. McGuire, E. Harley, L. E. McNeil, R. Khanna, S. J. Pearton, and J. M. Zavada, "Properties and annealing stability of Fe doped semi-insulating GaN structures," *Phys. Stat. Sol. (c)*, vol. 2, pp. 2476-2479, 2005.

[23] T. Aggerstam, A. Pinos, S. Marcinkevicius, M. Linnarsson, and S. Lourdudoss, "Electron and hole capture cross-sections of Fe acceptors in GaN : Fe epitaxially grown on sapphire," *J. Electronic Mater.*, vol. 36, pp. 1621-1624, Dec 2007.

[24] P. B. Klein, J. A. Freitas, Jr., S. C. Binari, and A. E. Wickenden, "Observation of deep traps responsible for current collapse in GaN metal-semiconductor field-effect transistors," *Appl. Phys. Lett.*, vol. 75, pp. 4016-18, 1999.

[25] J. L. Lyons, A. Janotti, and C. G. Van de Walle, "Carbon impurities and the yellow luminescence in GaN," *Appl. Phys. Lett.*, vol. 97, p. 152108, 2010.